

# FMODetect: Robust Detection and Trajectory Estimation of Fast Moving Objects

Denys Rozumnyi<sup>1,4</sup> Jiří Matas<sup>4</sup> Filip Šroubek<sup>2</sup> Marc Pollefeys<sup>1,3</sup> Martin Oswald<sup>1</sup>

<sup>1</sup>Department of Computer Science, ETH Zurich <sup>3</sup>Microsoft Mixed Reality and AI Zurich Lab  
<sup>2</sup>UTIA, Czech Academy of Sciences <sup>4</sup>Visual Recognition Group, Czech Technical University in Prague

## Abstract

*We propose the first learning-based approach for detection and trajectory estimation of fast moving objects. Such objects are highly blurred and move over large distances within one video frame. Fast moving objects are associated with a deblurring and matting problem, also called deblatting. Instead of solving the complex deblatting problem jointly, we split the problem into matting and deblurring and solve them separately. The proposed method first detects all fast moving objects as a truncated distance function to the trajectory. Subsequently, a matting and fitting network for each detected object estimates the object trajectory and its blurred appearance without background. For the sharp appearance estimation, we propose an energy minimization based deblurring. The state-of-the-art methods are outperformed in terms of trajectory estimation and sharp appearance reconstruction. Compared to other methods, such as deblatting, the inference is of several orders of magnitude faster and allows applications such as real-time fast moving object detection and retrieval in large video collections.*

## 1. Introduction

Fast moving objects (FMOs) are objects which look significantly blurred in images. In a single frame, they move at high speed over distances larger than their size. FMOs typically appear as blurred streaks formed as a composition of the background and their blurred appearance. Other scenarios include fast rotations of objects as a ceiling fan or a propeller. Fast moving objects are common in everyday scenarios like fast cars, falling objects, flying insects, rain, or hailstorm. They are mainly present in sports videos, such as tennis, football, volleyball, badminton, or any other game involving moving objects. Applications of FMO detection methods are temporal super-resolution, speed measurement, FMO retrieval, removal, and highlighting.

FMOs were introduced in [25], where the authors created the first dataset containing fast moving objects and proposed a proof-of-concept algorithm to detect and track such objects. The problem of detecting and tracking FMOs has been unnoticed by the research community, and such objects are not present in standard tracking datasets such as VOT [16], OTB [29] and ALOV [27]. More precisely, they may or may not be present, but FMO is never the object intended for tracking by the ground truth annotation. We highlight this by running FMO retrieval by the proposed method and detect FMOs in very recent standard large datasets like GOT-10k [8] and LaSOT [5] and find unannotated FMOs (Fig. 2). The former contains more than 10000 video segments with 1.5M manually labeled bounding boxes, and the latter contains 1400 sequences with more than 3.5M frames in total. By processing the ground truth bounding boxes in more than 5M frames from both datasets, we noticed that there is a significant overlap between consecutive bounding boxes in almost all cases, and the speed is close to zero (Fig. 2). In contrast, the recently proposed TbD dataset [14] with fast moving objects has almost zero intersection over union between consecutive objects, and the speed is higher.

Apart from [25], there are just a few published methods that deal with FMOs, such as Tracking by Deblatting (TbD) [14, 24]. TbD solves an inverse problem of deblurring and matting, hence *deblatting*, and decouples the input images into trajectory, appearance and mask. All previously published methods were based on classical energy minimization methods. While powerful, they still require many parameter tuning and are slow. In most cases, they have to be tuned for different sequences separately. Also, their performance is not entirely satisfactory, and they force several limiting assumptions, *e.g.* static camera, high contrast between the object and the background and spherical shape.

This paper proposes a novel method for FMO detection and trajectory and appearance estimation using a combina-



Figure 1. Examples of fast moving object (FMO) retrieval on YouTube videos by our method running in real-time. **Top:** frames from a 10-minute surveillance footage [[youtu.be/CkVJyAKwByw](https://youtu.be/CkVJyAKwByw)]. **Bottom:** frames from a 5-minute trick-shot video [[youtu.be/A2FsgKoGD04](https://youtu.be/A2FsgKoGD04)]. For each image, the detected FMO and its trajectory is shown as a red line in a close-up below. The object description contains a digitally clickable link to the timestamp when the event happened, in [minutes:seconds] format.

tion of deep learning and deblurring by energy minimization methods. Instead of solving an ill-posed and complex deblurring [14] problem, we first solve the matting problem, which separates the background from the input image by learning from synthetic data. Then, an easier deblurring problem is solved by energy minimization. The proposed FMODetect method is real-time capable and achieves state-of-the-art performance, which allows us to tackle challenging applications such as FMO retrieval and tracking in long videos, as illustrated in Fig. 1.

In summary, we make the following *contributions*:

- We present the first learned approach to the problem of FMO detection and trajectory estimation. By separating deblurring into matting and deblurring, computational and problem complexities are simplified, and the method achieves state-of-the-art results.
- Compared to previous work, the proposed method is simpler, does not require extensive parameter tuning, and works with the same settings for a wide range of scenarios, *e.g.* moving or zooming cameras, objects of different complexities and moving among various trajectories. The method is trained on a challenging synthetic dataset, which generalizes well to unseen and more difficult real-world data.
- Our method is real-time capable and more than an order of magnitude faster than the previous work. This

makes applications such as robust FMO retrieval from large video collections realistic.

- For the sharp appearance estimation, we propose a novel energy minimization based deblurring.
- We introduce a new synthetic dataset with fast moving objects used for training, which will be made publicly available together with the source code of this work.

## 2. Related work

The pioneering work in [25] introduced FMOs but was limited by many assumptions such as a linear trajectory, high contrast, and no occlusions. Some of them have been addressed in the follow-up method called Tracking by Deblurring (TbD) [14]. TbD solves an inverse problem of *deblurring* and *matting* by alternating iterative minimization, followed by fitting piecewise parabolic curves. As a by-product, TbD estimates sharp 2D object appearance, which is used for long-term tracking of fast moving objects. Both methods introduced datasets with fast moving objects. The ground truth in the FMO dataset [25] was only a binary mask with rough locations of FMOs in each frame. The TbD dataset [14] provides more ground truth information from a high-speed camera, such as object templates and sub-frame object trajectories.

The above-mentioned methods assumed causal processing of video frames, which means that the trajectory at the

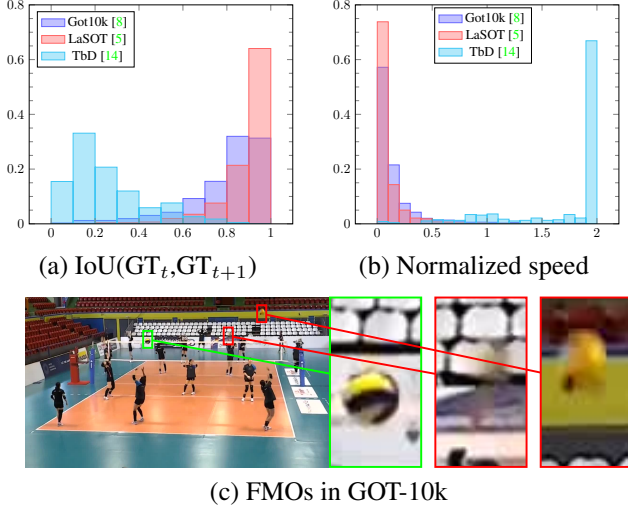


Figure 2. Histograms of (a) Intersection over Union (IoU) scores between consecutive ground truth bounding boxes and (b) speed normalized by the object size for datasets GOT-10k [8], LaSOT [5] and TbD [14], which focuses on FMOs. FMOs are present in GOT-10k and LaSOT datasets, but never annotated, *i.e.* trackers are not tested on fast moving objects. (c) Green box marks the annotated object in GOT-10k which is not an FMO, red boxes show unannotated FMOs retrieved by the proposed method.

current frame is estimated using only information from previous frames. However, most scenarios involving fast moving objects do not require causal processing, and some latency is acceptable. Non-causal Tracking by Deblatting (TbD-NC) [24] is the first method to exploit this fact. TbD-NC takes detections in each frame from a causal method as input and produces a single trajectory for the whole sequence. Then, the final trajectory is a continuous, piecewise polynomial curve. TbD-NC improves the accuracy and recall of trajectory estimation of fast moving objects. Also, it allows for accurate speed estimation, which is on par with expensive radar guns used in professional tennis matches. Applications such as temporal super-resolution become impressive with non-causal estimation.

The method proposed in this paper is causal, and computations are done for each frame independently. Therefore, the method in TbD-NC can be applied to improve the trajectories estimated by the proposed method.

The authors in [25] introduced fast moving objects together with the corresponding image formation model

$$I = H * F + (1 - H * M)B, \quad (1)$$

where the image is formed as a mixture of blurred object appearance and the background. Motion blur is modeled by the convolution of the object trajectory, represented by the blur kernel  $H$ , and the sharp object appearance  $F$ . The influence of background depends on the indicator function  $M$  of appearance  $F$ . For more details, the reader is referred

to [25].

Many deblurring methods have been proposed. They all assume small motions like in [11, 19, 22]. The method in [21] considers larger motions but only in a trivial case. We tried several of these methods, and none was able to deblur or reconstruct fast moving objects. Special deblurring of fast moving objects is also proposed in [13, 15, 28], but only a simple case is studied. The only competitive method is TbD [14]. TbD-3D [26] is an extension towards 3D objects with 3D rotations, which can be directly applied to the output of the proposed method.

Network architectures similar to the proposed one have been used in other methods. Hou *et al.* [7] proposed a two-encoder-two-decoder architecture but matting of sharp images is considered, as well as in [30, 33]. The architecture in [3] is similar, but the task is inverse – to synthesize the motion blur given sharp images. Similar U-Net [23] architectures have been applied in many image-to-image translation tasks [6, 10].

### 3. Method

The proposed method detects all fast moving objects in an image, recovers their trajectory, and removes the influence of the background, *i.e.* matting. Then an optional step is applied to get sharp object appearance, based on energy minimization based deblurring. An overview of the architecture is shown in Fig. 3.

First, an FMO detection network proposes potential regions with fast moving objects using a truncated distance function (TDF) to represent the trajectory. Second, for each region found by the detection network, the matting and fitting network estimates the parametric curve describing FMO trajectory and performs matting – removing the background from the input image and leaving only the blurred object appearance  $H * F$  and  $H * M$  from image formation model (1). This representation can be seen as an FMO moving in front of a completely black background. Estimating just  $H * F$  is not sufficient since the shape of the object should be estimated besides  $F$ , which models only the surface color. Consider an object of black color; here  $H * M$ , unlike  $H * F$ , is non-zero. The final step, deblurring, is done by energy minimization similar to deblatting [14]. However, by first removing the blended background, it is easier and faster.

#### 3.1. Detection network

The inputs to the detection network are the input image  $I$  and the background  $B$ , estimated as a median of the last three frames in a video sequence. The output is the truncated distance function  $D$ , measuring the distance to the object trajectory. If we assume that pixels are in some domain  $\mathbb{X} \subset \mathbb{R}^2$ , then for each pixel  $x \in \mathbb{X}$ ,  $D$  is defined as



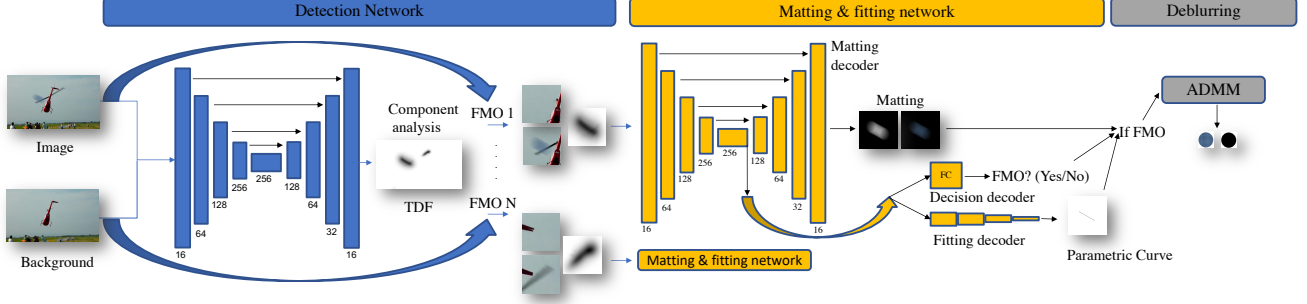


Figure 3. First, the FMO detection network performs the initial step to recover all fast moving objects (FMOs). Then, the matting and fitting network is applied on each detected FMO – a connected component in the binarized TDF. The outputs, blurred object without background and its trajectory, are then further used in the proposed deblurring (6) to establish sharp object appearance.

$$D(x) = 1 - \min(1, \min_t \frac{\|x - C(t)\|_2}{2r}), \quad (2)$$

where  $C(t) : [0, 1] \rightarrow \mathbb{R}^2$  is the ground truth continuous trajectory, and  $r$  is the ground truth object radius.

The ground truth for the training sequences is prepared as follows. First, a distance function to the trajectory is computed. It is then divided by the object diameter – the maximum distance between any two points on the object. Note that the pixels influenced by the object are located at half diameter distance to the trajectory. However, the network converges much faster when a larger neighborhood is considered. Experiments confirmed that it is beneficial to invert the TDF output, *i.e.* 0 means maximum distance (the truncation level), and 1 means ‘on the trajectory.’ The network benefits from the fact that the output is expected to be zero at most locations, which is easier to predict.

The architecture is similar to U-Net [23], and it is fully convolutional. The encoder contains four blocks as in [3], each followed by a max-pooling layer. Each block is built from three convolution layers with filter size  $3 \times 3$ , followed by a Leaky ReLU [18] with slope 0.1. The decoder part also contains four blocks, each followed by a transposed convolution layer [31, 32]. Inputs and outputs are rescaled to the resolution of  $256 \times 512$  pixels, with zero mean and unit variance. The full-resolution images are used for testing.

The loss function for the detection network is defined as

$$\mathcal{L}_d = \frac{1}{N_1} \sum_{D(x) > 0} \|D(x) - \hat{D}(x)\|_1 + \frac{1}{N_0} \sum_{D(x) = 0} \|\hat{D}(x)\|_1, \quad (3)$$

where  $D$  corresponds to the ground truth TDF, and  $\hat{D}$  to the estimated.  $N_1$  is the number of positive pixels in the ground truth TDF, and  $N_0$  is the number of zero value pixels where a fast moving object is not present in the neighborhood.

### 3.2. Matting and fitting network

The output  $D$  of the detection network is binarized by the threshold value  $\epsilon$ , and all connected components are extracted. For each connected component, we take crops from the input image, the background, and the non-binarized TDF. They are all scaled to the same resolution of  $256 \times 256$  pixels and are inputs to the network. The matting and fitting network output is three-fold: blurred object appearance without the influence of the background (matting), parametric trajectory and a binary decision whether the crop corresponds to the fast moving object. The last binary output is used to correct the mistakes of the detection network.

The matting and fitting network has a one-encoder-three-decoder architecture. The architecture is similar to the detection network. The transposed convolution operators are replaced by upsampling operators to avoid checkerboard artifact [20]. The output of the matting decoder is a 4-channel image ( $H \times F, H \times M$ ), since  $F$  is an RGB image and  $M$  is a gray-scale image. The fitting decoder performs further downsampling from the latent space until the output has only 8 channels: the degree of freedom of the estimated parametric trajectory. The last decoder contains only one fully connected layer attached to the latent space and is followed by a sigmoid activation with just a single output.

We assume that the trajectory within a frame is either a line or parabola or a piece-wise line with one bounce. Then, a common parametric representation of these three cases is the following

$$\mathcal{C}(t) = c_0 + c_1 \min(2t, 1) + c_2 \min(2t, 1)^2 + c_3 \max(2t - 1, 0), \quad \text{s.t. } 0 \leq t \leq 1, \quad (4)$$

where parameters  $c_k \in \mathbb{R}^2$ . In case of a line, parameters  $c_2$  and  $c_3$  are equal to zero vectors. In case of a parabola, only  $c_3$  is zero, and for a piece-wise line  $c_2$  is equal to zero. This parametrization can also represent a parabolic curve with a linear tail. However, to avoid this case, whenever  $\|c_3\| > 1$ , we set  $c_2$  to zero, otherwise  $c_3$  is set to zero.



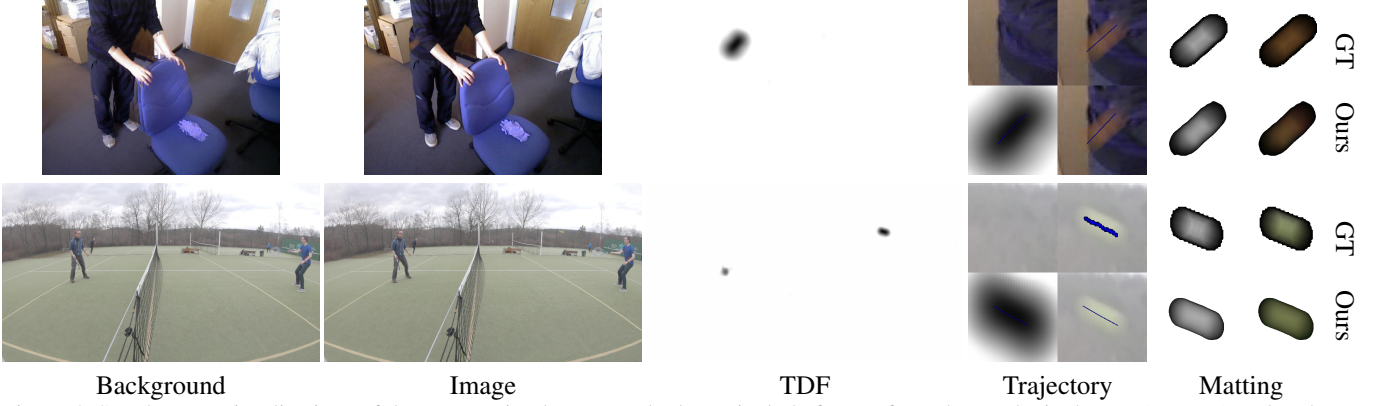


Figure 4. Step by step visualizations of data processing by our method. We include frames from the synthetic dataset (top row) and real-world TbD dataset [14] (bottom row). TDF stands for *truncated distance function* which is an intermediate output of our method for a detected trajectory. Trajectory reconstruction is plotted on the crops. Examples of deblurring after matting are shown in Fig. 5.

The loss function of the matting and fitting network is

$$\mathcal{L} = \alpha_a b (\|H * F - \hat{H}_F\|_1 + \|H * M - \hat{H}_M\|_1) + \alpha_c b \mathcal{L}_c(\mathcal{C}, \hat{\mathcal{C}}) + \alpha_b \text{BCE}(b, \hat{b}), \quad (5)$$

which combines three terms. The first one corresponds to blurred appearance reconstruction represented by the ground-truth pair  $(H * F, H * M)$ . The networks estimates are  $(\hat{H}_F, \hat{H}_M)$ . The second term penalizes deviations from the ground truth trajectory by the curve loss function  $\mathcal{L}_c$  which samples the trajectory at three points and computes an average distance between each pair. Since the direction is not known, we compute both options and choose the one with the minimal distance. The last term computes binary cross entropy between the estimated and the ground truth binary variable  $b$  which indicates whether the crop contains an FMO. All previous terms are multiplied by the ground truth binary variable to allow the network to output the best guess of trajectory and appearance even when there is no fast moving object, penalizing only for the incorrectly estimated binary variable  $b$ .

### 3.3. Deblurring

We formulate deblurring as an optimization problem. The output  $\hat{\mathcal{C}}$  of the fitting decoder is used for initialization. We also include optimization with respect to  $H$  in deblurring to account for small inaccuracies in the blur kernel. The object appearance and mask are then estimated by solving

$$\min_{F, M, H} \frac{1}{2} \left( \|H * F - \hat{H}_F\|_2^2 + \|H * M - \hat{H}_M\|_2^2 \right) + \alpha_F \|\nabla F\|_1 + \alpha_M \|\nabla M\|_1 \quad (6)$$

s.t.  $0 \leq F \leq M \leq 1$ ,  $H \geq 0$  and  $\sum_i H_i = 1$ . The deblurring inputs are  $\hat{H}_F$  and  $\hat{H}_M$ , which are the outputs of the matting decoder. All constraints are convex sets and we solve the problem using the alternating direction method of

multipliers [2]. The variables are split into blur kernel  $H$  and appearance model  $(F, M)$ , and both are updated iteratively. In case a parametric curve from  $H$  is needed, e.g. for evaluation, we run curve fitting from [14].

The deblurring problem (6) is much easier to solve than the deblatting problem [14]. Deblurring provides more accurate results, as illustrated in several examples in Fig. 5. It is twice faster than deblatting, and if minimization with respect to  $H$  is omitted from (6), it is 10 times faster.

Among other limitations of deblatting, which are solved by the proposed approach, are also failures to separate the background or a shadow correctly (Fig. 5, golf) or to deal with low contrast objects (Fig. 5, softball).

### 3.4. Training

The standard datasets with FMOs are the TbD [14] and FMO [25] datasets. Both are small, and the ground truth trajectories are estimated by running a state-of-the-art tracking algorithm on high-speed camera footage where the blur is not present. Since the ground truth of matting is not available and it not realistic to get, we create a new synthetic dataset with fast moving objects, called VOT-FMO. The VOT-FMO dataset is based on the VOT dataset [17], which is a standard dataset used in the tracking community. As previously shown in [25] and in Fig. 2, standard tracking datasets do not label fast moving objects, even though they still may be present there. Thus, the synthetic dataset is created by applying the FMO formation model (1) with backgrounds taken from the VOT dataset and with artificially inserted FMOs. Artificial FMOs are random discs of up to 100 pixels in radius with textures generated by GeoPatterns<sup>1</sup>. We generate 5000 random frames for training and 500 for validation.

Weights for the loss are set empirically:  $\alpha_a = 15$ ,  $\alpha_b = 0.4$ . Parameter  $\alpha_c$  is set to  $\frac{4}{256}$ , which normalizes the

<sup>1</sup><https://github.com/jasonlong-geo-pattern>

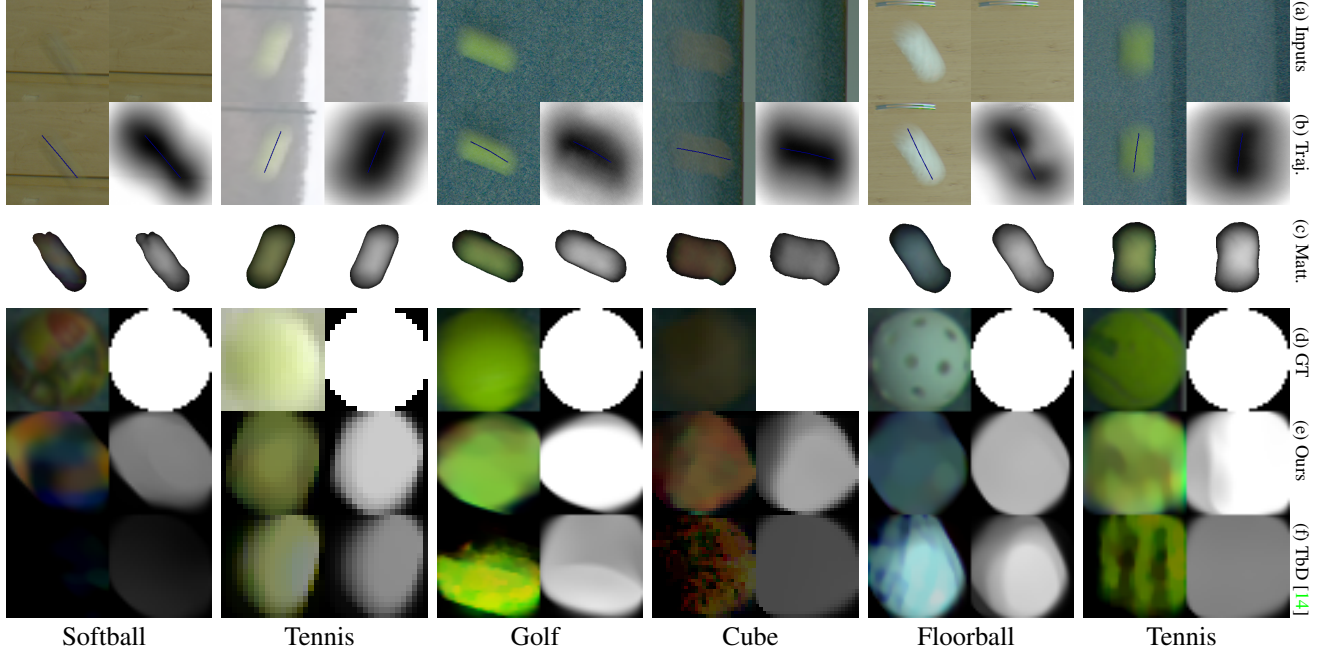


Figure 5. Matting and deblurring of fast moving objects in the TbD dataset [14] using the proposed method, and compared to deblatting [14]. From top to bottom: (a) inputs are image and the background by median, (b) left: estimated trajectory plotted on the input image, right: estimated truncated distance function (TDF), (c) output of the matting decoder, (d) ground truth (GT), (e) the proposed deblurring, and (f) deblatting [14].

curve loss to produce one unit when the average distance between trajectories is  $\frac{1}{4}$  of the crop width of 256 pixels. Regularization weights for deblurring were experimentally set to  $\alpha_F = 0.001$  and  $\alpha_M = 0.05$ . We found that the value of the binarization threshold  $\epsilon$  between 0.1 and 0.4 gives similar results. For experiments, we set it to 0.3.

The networks are trained by minimizing the joint loss function (sum) using Adam optimizer [12] with learning rate 0.00002. Batch normalization [9] is not used since it did not improve the results in our experiments. The implementation is written in Python using Keras [4] framework with Tensorflow [1] backend. The detection network contains 4.8M parameters, whereas the matting and fitting network contains 5.7M parameters. Training of both networks takes around three days on Nvidia GTX 1080 Ti GPU with 11 GB memory. The inference takes on average about 0.05 seconds on a single image of 600 by 960 pixels, which shows the real-time capability of the proposed method. In comparison, the previous methods [14, 24, 25] required a couple of seconds per frame on average.

## 4. Experiments

We evaluated the trajectory estimation on two datasets – TbD [14] and FMO [25]. In both cases, the compared methods are the FMO [25], TbD [14], and TbD-NC [24]. For the proposed FMODetect method, we report results for three ablated versions. The first version detects all FMOs and

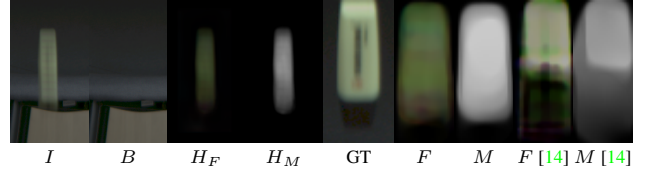


Figure 6. Additional deblurring results on a non-spherical object. From left to right: input image  $I$ , background  $B$ , estimated  $H_F$  and  $H_M$  by the matting decoder (removed background), the ground truth from a high-speed camera, object appearance  $F$  and mask  $M$  estimated by the proposed deblurring, and compared to reconstructions by the deblatting method [14].

estimates trajectories in real-time by the matting and fitting network. The second version additionally runs the proposed deblurring and further improves the trajectories without changing the recall. The last version uses the non-causal post-processing from TbD-NC [24] to complete missing detections and makes trajectories more consistent within the whole sequence.

### 4.1. TbD dataset

The TbD dataset [14] is a real-world dataset with FMOs, where ground truth object trajectory and appearance is available. Standard score measured on this dataset is Trajectory Intersection over Union (TIOU) which is defined [14]

Sequence	#	Baselines						Proposed					
		FMO [25]		TbD [14]		TbD-NC [24]		(a) Real-time		(b) + deblur.		(c) + NC	
		TIoU	Recall	TIoU	Recall	TIoU	Recall	TIoU	Recall	TIoU	Recall	TIoU	Recall
badm._w	40	0.242	0.34	<b>0.694</b>	<b>0.97</b>	<b>0.783</b>	<b>1.00</b>	0.210	0.94	0.684	0.94	0.749	0.95
badm._y	57	0.236	0.31	<b>0.677</b>	<b>0.91</b>	<b>0.780</b>	<b>1.00</b>	0.380	0.84	0.676	0.84	0.745	0.95
pingpong	58	0.064	0.12	0.523	<b>0.91</b>	0.643	<b>1.00</b>	0.302	0.87	<b>0.578</b>	0.87	<b>0.656</b>	0.92
tennis	38	0.596	0.78	0.673	0.97	0.750	<b>1.00</b>	0.588	<b>1.00</b>	<b>0.741</b>	<b>1.00</b>	<b>0.781</b>	<b>1.00</b>
volleyball	41	0.537	0.72	<b>0.795</b>	<b>0.97</b>	<b>0.857</b>	<b>1.00</b>	0.465	0.95	0.632	0.95	0.761	<b>1.00</b>
thr._floor	40	0.272	0.37	<b>0.810</b>	<b>1.00</b>	<b>0.855</b>	<b>1.00</b>	0.430	<b>1.00</b>	0.736	<b>1.00</b>	0.809	<b>1.00</b>
thr._soft	60	0.377	0.57	0.652	0.97	<b>0.761</b>	<b>1.00</b>	0.470	<b>1.00</b>	<b>0.658</b>	<b>1.00</b>	0.748	<b>1.00</b>
thr._ten.	45	0.507	0.65	0.850	<b>1.00</b>	0.878	<b>1.00</b>	0.623	<b>1.00</b>	<b>0.856</b>	<b>1.00</b>	<b>0.907</b>	<b>1.00</b>
roll_golf	16	0.187	0.71	<b>0.873</b>	<b>1.00</b>	0.894	<b>1.00</b>	0.681	<b>1.00</b>	0.846	<b>1.00</b>	<b>0.895</b>	<b>1.00</b>
fall_cube	20	0.408	0.78	<b>0.721</b>	<b>1.00</b>	<b>0.757</b>	<b>1.00</b>	0.602	<b>1.00</b>	0.708	<b>1.00</b>	<b>0.757</b>	<b>1.00</b>
hit.ten.	30	0.381	0.68	0.667	0.93	0.714	<b>1.00</b>	0.748	<b>1.00</b>	<b>0.743</b>	<b>1.00</b>	<b>0.770</b>	<b>1.00</b>
hit.ten.2	26	0.414	0.71	0.616	0.83	0.682	0.92	0.730	<b>1.00</b>	<b>0.734</b>	<b>1.00</b>	<b>0.791</b>	<b>1.00</b>
Average	39	0.352	0.56	0.713	0.96	0.779	<b>0.99</b>	0.519	0.97	<b>0.715</b>	<b>0.97</b>	<b>0.781</b>	<b>0.99</b>
Runtime		1 fps		0.2 fps		N/A		20 fps		0.4 fps		N/A	

Table 1. TIoU (7) and recall on the TbD dataset – comparison of the proposed methods to the baselines: FMO method [25], TbD [14] and TbD-NC [24] methods. Ablated versions of the proposed method: (a) real-time with trajectories estimated by the network, (b) with the proposed deblurring, and (c) with non-causal post-processing from [24]. For each sequence, the highest TIoU and recall are highlighted in **bold** font. The comparison between the best-performing causal method is colored by **dark blue**. Qualitative comparison is in Fig. 7.

Method	FMO method	TbD	TbD-NC	Ours
Precision	59.2	81.6	83.4	<b>84.9</b>
Recall	35.5	41.1	45.1	<b>48.8</b>

Table 2. Precision and recall, averaged on the 16 sequences of the FMO dataset [25]. The proposed method (real-time version) outperforms both the causal TbD method [14] and the global non-causal TbD-NC method [24].

as

$$\text{TIoU}(\mathcal{C}, \mathcal{C}^*) = \int_t \text{IoU} \left( M_{\mathcal{C}(t)}^*, M_{\mathcal{C}^*(t)}^* \right) dt, \quad (7)$$

where object mask is placed on a trajectory point  $\mathcal{C}(t)$ , denoted by  $M_{\mathcal{C}(t)}^*$ , and the standard Intersection over Union (IoU) is computed. Then the average is calculated along the whole trajectory.

The accuracy of the trajectory reconstruction is shown in Table 1. The real-time version of our method is on par with other causal baselines in terms of recall. However, it is in orders of magnitude faster, which comes at the cost of less precisely localized trajectories measured by TIoU. FMOdetect with deblurring outperforms TbD, and even approaches on some sequences TbD-NC, which is a non-causal method. The best scores are achieved when the non-causal post-processing is added to the proposed method (Fig. 7), and it is the best-performing method.

## 4.2. FMO dataset

The FMO dataset [25] does not contain ground truth trajectories nor sharp object appearances. The only provided ground truth is a binary region where the fast moving object is located. The authors report only precision, recall, and F-score for the evaluation. FMOdetect outperforms all other methods on this dataset (Table 2).

## 4.3. Model generalization

As shown in the experiments, the method works well on real data, even when trained on synthetic. In Fig. 4 we visualize outputs of the detection network on the full resolution. The estimated TDFs are correct for both synthetic and real data. The method has only seen synthetic FMOs with spherical shape in the training examples, but FMOs of more complex shapes can also be detected. The first example is the FMO retrieval experiment (Fig. 1) of two YouTube videos, where highly complex objects (a hand, a cap, or a keychain) are successfully detected. The second example is in Fig. 5 of a thrown wooden cube. The detection network correctly estimates the TDF, and then the fitting decoder outputs a precise trajectory, and finally, the matting decoder successfully removes the background. This is checked by further applying the proposed deblurring, which outputs object appearance that resembles a cube. In comparison, the output of deblatting [14] is poor, and the cubic shape is not visible there. Similar results can be seen in Fig. 6.

FMOdetect can also handle situations with a moving or



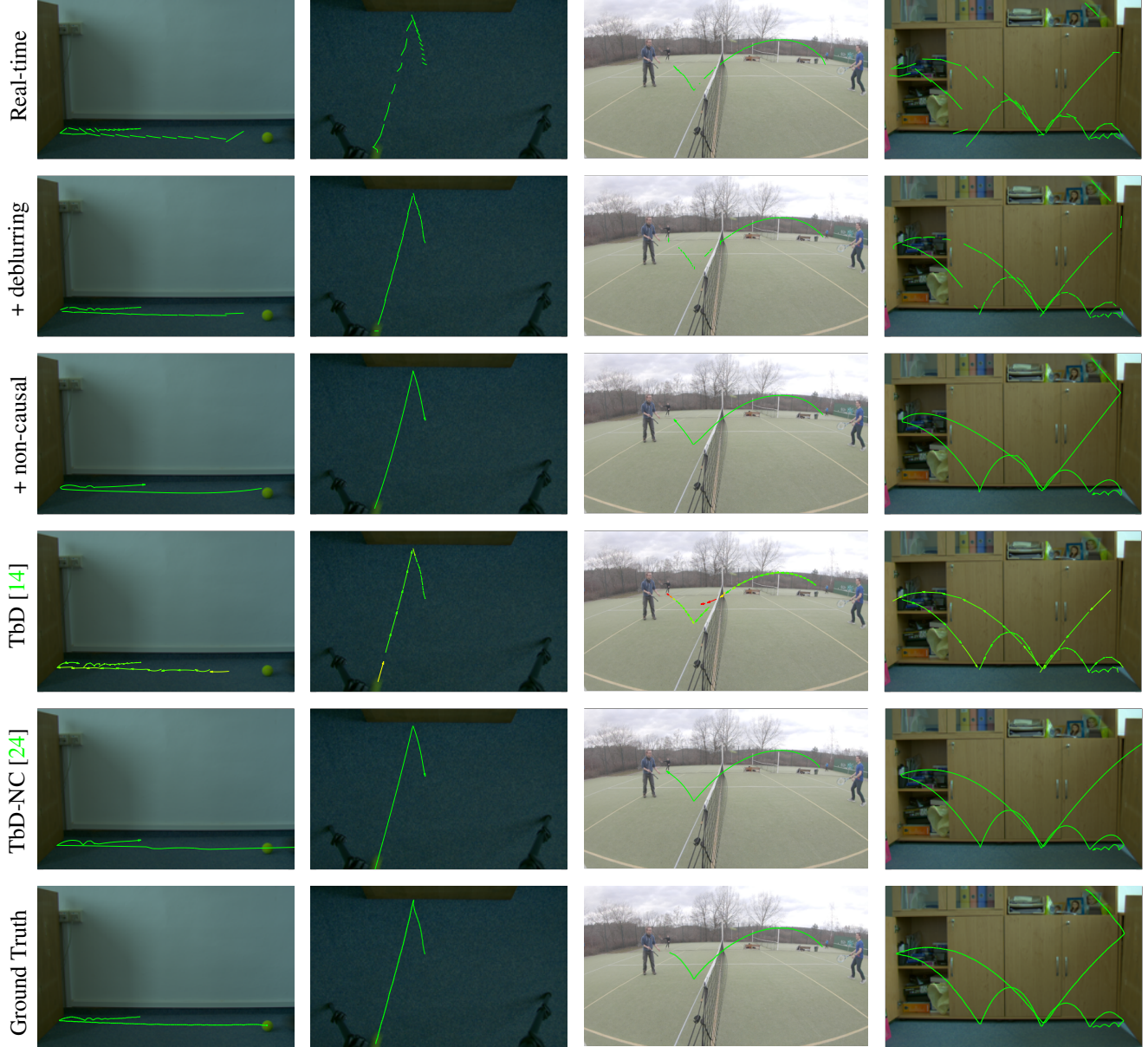


Figure 7. Trajectory estimation on four sequences from the TbD dataset by the proposed method compared to state-of-the-art methods. From top to bottom: real-time version of the proposed method, with deblurring, with deblurring and non-causal post-processing from [24], TbD [14], TbD-NC [24], the ground truth.

zooming camera (Fig. 1), as videos in the VOT dataset used for training contain similar types of camera motion. Compared to the previous methods [14, 24], which all require an initial detection by an FMO detector [25] for further tracking, and which fail to detect objects with low contrast (such as the softball in Fig. 5), the proposed method succeeds in this task as there was no restriction on the contrast in the synthetic dataset.

Among drawbacks of the proposed method are failures on irregular motions, *e.g.* the ceiling fan in Fig. 2, since the

synthesized dataset has no such motions.

## 5. Conclusion

We proposed the first learning-based method for fast moving object detection and trajectory reconstruction. FMODetect improves precision, robustness, and computation time compared to previous methods. In terms of trajectory estimation, we achieve state-of-the-art results on two benchmark datasets. By simplifying deblatting into matting and deblurring, we estimate appearance using energy

minimization and produce qualitatively better results than deblatting. The proposed method is real-time capable and an order of magnitude faster than previous FMO detection methods. This allows for realistic applications such as efficient FMO scanning or retrieval in large video collections.

## References

- [1] Martín Abadi, Ashish Agarwal, Paul Barham, Eugene Brevdo, Zhifeng Chen, Craig Citro, Greg S. Corrado, Andy Davis, et al. TensorFlow: Large-scale machine learning on heterogeneous systems, 2015. Software available from tensorflow.org. **6**
- [2] Stephen Boyd, Neal Parikh, Eric Chu, Borja Peleato, and Jonathan Eckstein. Distributed optimization and statistical learning via the alternating direction method of multipliers. *Foundations and Trends in Machine Learning*, 3(1):1–122, Jan. 2011. **5**
- [3] T. Brooks and J. T. Barron. Learning to synthesize motion blur. In *CVPR*, pages 6833–6841, June 2019. **3, 4**
- [4] François Chollet. keras. <https://github.com/fchollet/keras>, 2015. **6**
- [5] H. Fan, L. Lin, F. Yang, P. Chu, G. Deng, S. Yu, H. Bai, Y. Xu, C. Liao, and H. Ling. Lasot: A high-quality benchmark for large-scale single object tracking. In *CVPR*, pages 5369–5378, June 2019. **1, 3**
- [6] Abel Gonzalez-Garcia, Joost van de Weijer, and Yoshua Bengio. Image-to-image translation for cross-domain disentanglement. In *NeurIPS*, page 1294–1305, Red Hook, NY, USA, 2018. Curran Associates Inc. **3**
- [7] Qiqi Hou and Feng Liu. Context-aware image matting for simultaneous foreground and alpha estimation. In *ICCV*, October 2019. **3**
- [8] Lianghua Huang, Xin Zhao, and Kaiqi Huang. Got-10k: A large high-diversity benchmark for generic object tracking in the wild. *IEEE TPAMI*, page 1–1, 2019. **1, 3**
- [9] Sergey Ioffe and Christian Szegedy. Batch normalization: Accelerating deep network training by reducing internal covariate shift. In *ICML*, page 448–456. JMLR.org, 2015. **6**
- [10] P. Isola, J. Zhu, T. Zhou, and A. A. Efros. Image-to-image translation with conditional adversarial networks. In *CVPR*, pages 5967–5976, July 2017. **3**
- [11] Meiguang Jin, Givi Meishvili, and Paolo Favaro. Learning to extract a video sequence from a single motion-blurred image. In *CVPR*, June 2018. **3**
- [12] Diederik P. Kingma and Jimmy Ba. Adam: A method for stochastic optimization. In Yoshua Bengio and Yann LeCun, editors, *ICLR*, 2015. **6**
- [13] J. Kotera, J. Matas, and F. Šroubek. Restoration of fast moving objects. *IEEE TIP*, 29:8577–8589, 2020. **3**
- [14] J. Kotera, D. Rozumnyi, F. Šroubek, and J. Matas. Intra-frame object tracking by deblatting. In *ICCVW*, Oct 2019. **1, 2, 3, 5, 6, 7, 8**
- [15] J. Kotera and F. Šroubek. Motion estimation and deblurring of fast moving objects. In *ICIP*, pages 2860–2864, Oct 2018. **3**
- [16] Matej Kristan, Aleš Leonardis, Jiří Matas, Michael Felsberg, Roman Pflugfelder, Luka Čehovin, Tomáš Vojtík, Gustav Hager, Alan Lukežič, Gustavo Fernández, Abhinav Gupta, Alfredo Petrosino, Alireza Memarmoghdam, Alvaro Garcia-Martin, Andrés Solís Montero, Andrea Vedaldi, Andreas Robinson, and other. The visual object tracking vot2016 challenge results. In Gang Hua and Hervé Jégou, editors, *ECCVW*, pages 777–823, Cham, 2016. Springer International Publishing. **1**
- [17] Matej Kristan, Ales Leonardis, Jiri Matas, Michael Felsberg, Roman Pflugfelder, Luka Čehovin Zajc, Tomas Vojir, Goutam Bhat, Alan Lukežic, Abdelrahman Eldesokey, Gustavo Fernandez, and et al. The sixth visual object tracking vot2018 challenge results. In *ECCVW*, Sep 2018. **5**
- [18] Andrew L. Maas, Awni Y. Hannun, and Andrew Y. Ng. Rectifier nonlinearities improve neural network acoustic models. In *ICML Workshop on Deep Learning for Audio, Speech and Language Processing*, 2013. **4**
- [19] S. Nah, T. H. Kim, and K. M. Lee. Deep multi-scale convolutional neural network for dynamic scene deblurring. In *CVPR*, pages 257–265, July 2017. **3**
- [20] Augustus Odena, Vincent Dumoulin, and Chris Olah. Deconvolution and checkerboard artifacts. *Distill*, 2016. **4**
- [21] Liyuan Pan, Richard Hartley, Miaomiao Liu, and Yuchao Dai. Phase-only image based kernel estimation for single image blind deblurring. In *CVPR*, June 2019. **3**
- [22] Kuldeep Purohit, Anshul Shah, and A. N. Rajagopalan. Bringing alive blurred moments. In *CVPR*, June 2019. **3**
- [23] O. Ronneberger, P. Fischer, and T. Brox. U-net: Convolutional networks for biomedical image segmentation. In Nassir Navab, Joachim Hornegger, William M. Wells, and Alejandro F. Frangi, editors, *MICCAI*, pages 234–241, Cham, 2015. Springer International Publishing. **3, 4**
- [24] D. Rozumnyi, J. Kotera, F. Šroubek, and J. Matas. Non-causal tracking by deblatting. In Gernot A. Fink, Simone Frintrop, and Xiaoyi Jiang, editors, *GCPR*, pages 122–135, Cham, 2019. Springer International Publishing. **1, 3, 6, 7, 8**
- [25] D. Rozumnyi, J. Kotera, F. Šroubek, L. Novotný, and J. Matas. The world of fast moving objects. In *CVPR*, pages 4838–4846, July 2017. **1, 2, 3, 5, 6, 7, 8**
- [26] D. Rozumnyi, J. Kotera, F. Šroubek, and J. Matas. Sub-frame appearance and 6d pose estimation of fast moving objects. In *CVPR*, pages 6777–6785, 2020. **3**
- [27] A. W. M. Smeulders, D. M. Chu, R. Cucchiara, S. Calderara, A. Dehghan, and M. Shah. Visual tracking: An experimental survey. *IEEE TPAMI*, 36(7):1442–1468, July 2014. **1**
- [28] F. Šroubek and J. Kotera. Motion blur prior. In *ICIP*, pages 928–932, 2020. **3**
- [29] Yi Wu, Jongwoo Lim, and Ming-Hsuan Yang. Online object tracking: A benchmark. In *CVPR*, 2013. **1**
- [30] N. Xu, B. Price, S. Cohen, and T. Huang. Deep image matting. In *CVPR*, pages 311–320, July 2017. **3**
- [31] M. D. Zeiler, D. Krishnan, G. W. Taylor, and R. Fergus. Deconvolutional networks. In *CVPR*, pages 2528–2535, June 2010. **4**
- [32] M. D. Zeiler, G. W. Taylor, and R. Fergus. Adaptive deconvolutional networks for mid and high level feature learning. In *ICCV*, pages 2018–2025, Nov 2011. **4**

- [33] Y. Zhang, L. Gong, L. Fan, P. Ren, Q. Huang, H. Bao, and W. Xu. A late fusion cnn for digital matting. In *CVPR*, pages 7461–7470, June 2019. [3](#)